Dehydration Behavior of Eprosartan Mesylate Dihydrate

JIE SHENG,[†,‡] GOPADI M. VENKATESH,[§,||] SARMA P. DUDDU,[§,⊥] AND DAVID J. W. GRANT*[,†]

Contribution from *Department of Pharmaceutics, College of Pharmacy, University of Minnesota, Weaver-Densford Hall, 308 Harvard Street SE., Minneapolis, Minnesota 55455-0343 and SmithKline Beecham Pharmaceuticals R&D, Pharmaceutical Development Maildrop UP 1230, 1250 S. Collegeville Road, Collegeville, Pennsylvania 19426-0949.*

Received January 27, 1999. Final revised manuscript received July 7, 1999.
Accepted for publication July 19, 1999.

Abstract □ Eprosartan mesylate (SKF 108566-J; EM) is an antihypertensive agent approved for marketing in the USA. EM dihydrate was prepared by three methods, one of which included suspending the anhydrous drug in an aqueous solution of 1.0 M methanesulfonic acid to form a slurry, followed by filtration. The dehydration kinetics of EM dihydrate were derived by analyzing the fit of the isothermal thermogravimetric analytical (TGA) data to numerous kinetic models. EM dihydrate undergoes dehydration in two distinct steps, each involving the loss of 1 mol of water at 25–70 °C and 70–120 °C, respectively. Recrystallization of EM occurs at ∼120–140 °C after dehydration to the anhydrous phase. This explanation is supported by variable temperature powder X-ray diffractometry. The mechanism of the dehydration reaction is complex, the dependence of the reaction rate on temperature varying as a function of the particles size. For the dihydrate of sieve fraction <125 μm, the kinetics of the first and second dehydration steps are consistent with the Avrami–Erofeev equation (A3, $n = 1/3$) over the temperature range studied, corresponding to three-dimensional growth of nuclei. In contrast, for the 125–180-μm and 180–250-μm sieve fractions, the kinetics are best described by the two-dimensional phase boundary reaction (R2) at a lower dehydration temperature (i.e., 28.3 °C), and by the Avrami–Erofeev equation (A3, $n = 1/3$) at a higher dehydration temperature (i.e., 93.7 °C). The activation energies (15–40 kcal/mol) and frequency factors of the dehydration of EM dihydrate were determined both by Arrhenius plots of the isothermal rates determined by TGA and by Kissinger plots of the nonisothermal differential scanning calorimetric data. Hot stage microscopy of single crystals of EM dihydrate showed random nucleation at the surface and dehydration with the growth of microcrystals along the needle *a* axis. Cerius^{2TM} molecular modeling software showed the existence of water channels along the *a* axis and enabled the observed dehydration behavior of EM dihydrate crystals to be explained in terms of the bonding environment of water molecules in the crystal structure.

Introduction

The presence of water of hydration is common in molecular crystals of both organic and inorganic compounds. Numerous pharmaceuticals exist in both hydrated and anhydrous forms.[1,2] More than 90 hydrates are listed in the *United States Pharmacopoeia*,[3] and at least one-third of the solid crystalline substances of the *European Pharmacopoeia*[4] are reported to form hydrates. The stability and behavior of hydrates can vary widely,[5−7] and hydrate formation and dehydration may occur during processing or storage of pharmaceuticals. Knowledge of the hydration and dehydration behavior of drug substances is essential in the development of stable formulations because the physicochemical, mechanical, processing, and biological properties of hydrates can differ significantly from those of the corresponding anhydrate; these differences are ascribed to differences in crystal structure[7−14] brought about by the presence of lattice water. In general, water molecules in hydrates are almost always involved in hydrogen bonds that usually contribute to the coherence of the crystal structure. Shefter and Higuchi[13] found that the apparent dissolution rate and solubility of the anhydrous form of several drugs are greater than those of the hydrate, which crystallizes from water at the same temperature as in the dissolution experiments (e.g., theophylline, caffeine, and glutethimide). Poole et al.[14] showed that the enhanced bioavailability of ampicillin correlated positively with the greater aqueous solubility and dissolution rate of anhydrous ampicillin compared with that of the trihydrate form. Lerk et al. reported that the binding capacity and flowability of α-lactose monohydrate[15] and of α-D-glucose[16] increased after dehydration because of a difference in pore size distribution. Because the phase transition on hydration or dehydration is accompanied by a change in the physicochemical properties, it is important to understand the mechanisms of these transitions, the experimental and environmental conditions under which they take place, and their rates under various conditions.

Classic dehydration kinetics is treated as a solid-state reaction, as shown in eq 1.[7,17]

$$A{\cdot}H_2O\ (s) \rightarrow A\ (s) + H_2O\ (g) \qquad (1)$$

Usually, reactions involving solids start from the surface and proceed inward as the reactant−product boundary layer contracts.[18] The initial generation of small product crystallites at the reactant−product interface is termed nucleation.[19] Such nucleation is most likely to occur at surfaces, where the molecules are usually more energetic than in the bulk of the crystal.[20] For a reaction such as desolvation, which involves a single solid, nucleation may occur rapidly over all surfaces or at the points of initial contact between the constituents of a mixture of solids. Two general points should be taken into consideration for solid-state reactions. First, the reactivity of a solid substance is often dependent on the total concentrations of highly deformed, or defective, regions of the lattice. Damaged external surfaces, superficial lattice imperfections, and scratches are often chemically more reactive than more perfect crystal faces. Second, the kinetics of a solid-state reaction may be controlled by the surface area, which is related to the mean particle size and to the particle size

* Corresponding author. Telephone: (612) 624-3956. Facsimile: (612) 625−0609. E-mail: grant001@tc.umn.edu.
† Department of Pharmaceutics.
§ SmithKline Beecham Pharmaceuticals R&D.
‡ Present address: Lilly Research Laboratories, A Division of Eli Lilly and Company, Drop Code GL36, 2001 West Main Street, P.O. Box 708, Greenfield, Indiana 46140.
|| Eurand, 845 Center Drive, Vandalia, Ohio.
⊥ Inhale Therapeutic Systems, San Carlos, California 94070.

© 1999, American Chemical Society and American Pharmaceutical Association
10.1021/js9900250 CCC: $18.00
Published on Web 09/11/1999

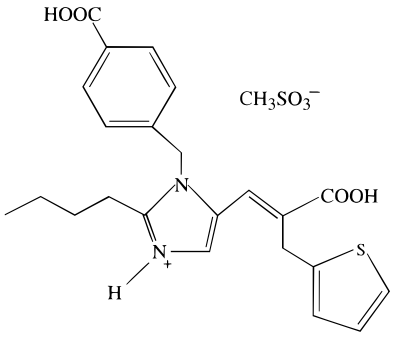

Scheme 1—The Molecular Structure of Eprosartan Mesylate (EM)

distribution. Because of the intrinsic heterogeneity of solid phases, the dehydration reaction is also sensitive to the environmental and reactant conditions, such as temperature, water vapor pressure, sample pre-history, sample weight,[21,22] and the geometry of the solid particles.[23]

Growth of nuclei in three dimensions has been observed during the decomposition of several compounds, but is not general because experimental observations for other substances have shown that the growth of nuclei under other conditions may be confined to particular lattice planes (i.e., along one or two dimensions).[19] Numerous methods have been used to study the dehydration process, including thermomicroscopy (hot stage microscopy, HSM), differential scanning calorimetry (DSC), thermogravimetric analysis (TGA), X-ray crystallography (powder X-ray diffractometry, PXRD), and analysis of the evolved gases.[7] The experimental dehydrated fraction, x, at different times, t, is plotted against t according to the kinetic models of the reaction mechanisms that are capable of operating in the solid-state decomposition.[18,24,25] The goodness of the fit to each kinetic equation was derived by examining the scatter of the residuals, s_e, about the mean, the standard deviation of the regression, S, and the determination coefficient, R^2, with less emphasis on the latter. Davis and Pryor[26] and Brown and Galwey[27] have criticized the use of R^2 alone as the sole determinant of the kinetic equation of best fit, especially when it has similar values for closely related equations. Random s_e without a trend and relatively small values of S of the regression are required for demonstrating a good fit to any reasonable kinetic model.[21,26] However, a good fit to a particular equation does not necessarily imply that the corresponding mechanism is correct.

Eprosartan mesylate (EM, Scheme 1) is used in the treatment of hypertension and exists as a dihydrate and anhydrate.[28,29] EM dihydrate can be prepared under a variety of conditions, for examples, by exposing the anhydrous drug substance to 98% RH for >15 days, by suspending the drug in an aqueous solution of 1.0 M methanesulfonic acid to form a slurry, and by granulating the drug in the presence of 3% corn starch. Little work has been done to study the dehydration behavior and kinetics of EM dihydrate, which is the basic information required for predicting the stability and other physicochemical properties of EM tablets. The purpose of this paper is to elucidate the dehydration kinetics of EM dihydrate, especially the effects of the particle size and temperature. Variable temperature PXRD and HSM should help to justify a mechanistic interpretation of the data. Cerius^{2TM} molecular modeling was used to visualize the crystal packing and to provide insight into the dehydration process at the molecular level. Preliminary reports of this work have been presented at the 1997 Annual Meeting of the American Association of Pharmaceutical Scientists.[30,31]

Experimental Section

Materials—Eprosartan mesylate (EM) anhydrate was supplied by SmithKline Beecham Pharmaceuticals, King of Prussia, PA. Methanesulfonic acid used for the preparation of EM dihydrate was supplied by Aldrich Chemical Company, Milwaukee, WI.

Preparation of EM Dihydrate—EM dihydrate was prepared by suspending 1.6 g of the anhydrous drug in 40 mL of 1.0 M aqueous methanesulfonic acid (to prevent the formation of eprosartan free base and to reduce the solubility of the salt, EM dihydrate, by the common ion effect) at 22.5 °C (room temperature). The suspension was sonicated for 2 min at 22.5 °C, and was then stirred for 2 h. The solid phase was collected by filtration, thoroughly washed with distilled water at 0 °C, and dried for 48 h at 22.5 °C in a 58% RH chamber. EM dihydrate was also prepared by exposing the anhydrous drug to 98% RH at 45 °C for 15 days or longer and by granulating the anhydrous drug in the presence of 3% (w/w) corn starch and 10% (w/w) distilled water. The experimental techniques for solid-state characterization, described later, show that the materials prepared by each of the three methods (slurry process, exposure to 98% RH, or granulation with 3% (w/w) corn starch) are indeed the same phase of EM dihydrate. The crystals, prepared by each method, were fractionated using USP standard sieves into the following three particle size ranges: <125 μm, 125−180 μm, and 180−250 μm.

Differential Scanning Calorimetry (DSC)—A DuPont differential scanning calorimeter (model 910, TA Instruments, New Castle, DE) equipped with a data station (Thermal Analyst 2000, TA Instruments) was used for the nonisothermal DSC studies. The temperature axis and cell constant of the DSC cell were calibrated with indium. The sample (2.05 ± 0.02 mg) was heated in open pans at heating rates of 5, 10, 15, 20, 25, 30, and 35 °C/min under 300−400 mL/min nitrogen purge. The activation energy of each dehydration step was determined by Kissinger's method[32] in which the heating rate, ϕ in °C/min, and the temperature at peak maximum, T_m in degrees Kelvin, are plotted according to the eq 2. This equation is derived with the assumption that the rate of reaction is maximal at the temperature at which the endothermic peak reaches a maximum. The activation energy was calculated from the slopes of the plots of $\ln(\phi/T_m^2)$ versus $1/T_m$.

$$\mathrm{d}\ln(\phi/T_m^2)/\mathrm{d}(1/T_m) = -E_a/R \qquad (2)$$

Thermogravimetric Analysis (TGA)—A DuPont thermogravimetric analyzer (model 951, TA Instruments, New Castle, DE) linked to a data station (Thermal Analyst 2000, TA Instruments) was used for the isothermal dehydration studies. The weight loss, expressed as fraction dehydrated, x, at time t, was fitted to the known solid-state kinetic equations.[7,18,25] The activation energy and the frequency factor for the dehydration of EM dihydrate were calculated from the slope and the intercept, respectively, of the Arrhenius plots of the logarithm of the rate constants versus reciprocal absolute temperature. For the first dehydration step, corresponding to the formation of the monohydrate, isothermal scans of x versus t were obtained at fixed temperatures covering the range of 28 to 35 °C. The fraction dehydrated was calculated as the ratio, weight of water lost/maximum possible weight loss of water, in dehydrating EM dihydrate to the monohydrate. Therefore, 100% fraction dehydrated ($x = 1$) corresponds to the loss of 1 mol of water of hydration. For the second dehydration step, corresponding to the formation of the anhydrate from the monohydrate, the samples were heated in advance to 40 °C to allow completion of the first dehydration step. Analogous isothermal x versus t plots were obtained at fixed temperatures from 75 to 95 °C. Therefore, 100% fraction dehydrated ($x = 1$) corresponds the loss of 1 mol of water from EM monohydrate leading to the anhydrate. Prior to each isothermal scan, the sample (10.00 ± 0.02 mg) was rapidly heated to the set temperature at a rate of 150 °C/min and maintained at that temperature until the each dehydration step was completed. Nitrogen purge at a constant rate (300−400 mL/min) was maintained during each run.

Variable Temperature Powder X-ray Diffraction (PXRD)—Variable temperature PXRD of EM dihydrate was carried out at ambient temperature and atmosphere using a diffractometer (Scintag 2000, Sunnyvale, CA) with a hot stage attachment, with Cu Kα radiation (40 mA, 45 kV). Samples were packed in a copper

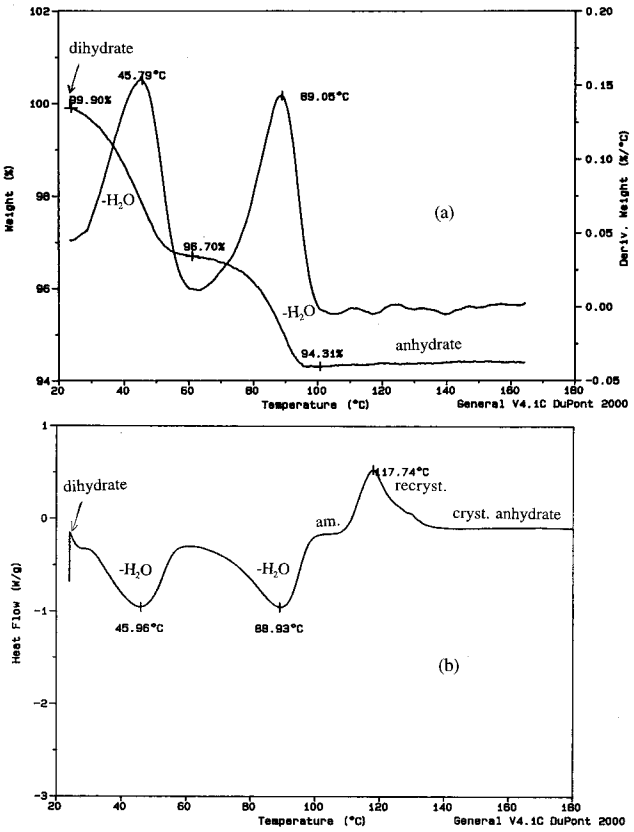

Figure 1—Typical curves for (a) thermogravimetric analysis (TGA), derivative thermogravimetric analysis (dTGA), and (b) differential scanning calorimetry (DSC) of eprosartan mesylate (EM) dihydrate.

holder and heated at the rate of 10 °C/min to the set temperature. The diffraction angle, 2θ, was scanned from 5° to 15° and increased at a rate of 3°/min with a counting time of 1 s.

Polarized Light Microscopy—EM dihydrate and the solid phase remaining after dehydration were observed under an optical microscope equipped with polarized light accessories (M3J, Wild Heerbrugg, Heerbrugg, Switzerland).

Hot Stage Microscopy (HSM)—The thermal events were observed on a hot stage (FP80, Mettler Instrument Corp., Highstown, NJ) under a microscope (M3J, Wild Heerbrugg, Heerbrugg, Switzerland). The EM dihydrate crystals were heated at a constant rate of 5 °C/min up to the melting point of anhydrous EM at ~250 °C.

Molecular Modeling—All molecular modeling calculations were performed using Cerius^{2TM} software, program version 3.5 (Molecular Simulations, San Diego, CA), running on the commercial workstations (Silicon Graphics, Personal Iris 4D/20, Power Series 2×R3000 and Indigo R4000).

Results and Discussions

Identification of Dehydration Steps—EM dihydrate exhibits two successive dehydration steps at 25−70 °C and 70−120 °C in open-pan TGA (Figure 1a), each corresponding to the loss of 1 mol of water. When EM dihydrate samples were subjected to DSC in an open pan under experimental conditions similar to those for TGA, the peak maximum temperatures in the DSC curve (46 °C and 89 °C in Figure 1b) agreed well with those in derivative TGA (dTGA) (46 °C and 89 °C in Figure 1a) for both dehydration steps. In addition, the DSC curve showed an exotherm with a peak maximum at 118 °C, suggesting recrystallization of EM anhydrate from the amorphous phase that was presumably formed immediately after the second dehydration step. These results were confirmed by variable temperature PXRD (Figure 2), despite the low signal-to-noise

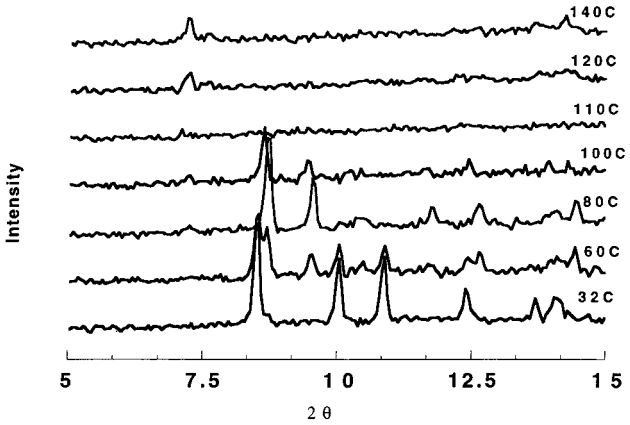

Figure 2—Variable temperature powder X-ray diffraction patterns for eprosartan mesylate (EM) dihydrate.

ratio, which is attributed to the small sample size and to the narrow range of scan angles. At 32 °C, EM dihydrate remains as its original form, as indicated by the PXRD pattern, which is similar to that of EM dihydrate (Figure 3a). As the temperature increases from 32 to 100 °C, the EM dihydrate gradually loses 1 mol of water to yield a mixture of the original dihydrate and a new phase, presumably the monohydrate, at 60 and 80 °C, and the monohydrate alone at 100 °C. Above 100 °C, the EM monohydrate gradually loses the final 1 mol of water and to form an amorphous phase, presumably that of EM anhydrate at 110 °C. At 150 °C, the PXRD pattern shows a new solid phase with low intensity peaks corresponding to a phase of low crystallinity, presumably the EM anhydrate that crystallized at ~118 °C in DSC (Figure 1b). Unlike the amorphous anhydrate, the partially crystalline anhydrate appeared birefringent under polarized light microscopy (Figure 4f). The phase changes of EM dihydrate on heating are summarized as follows:

first step dehydration:

$$\mathrm{EM{\cdot}2H_2O\ (crystal)} \xrightarrow{25-70\ ^\circ\mathrm{C}} \mathrm{EM{\cdot}H_2O\ (crystal)} + \mathrm{H_2O\ (g)}$$

second step dehydration:

$$\mathrm{EM{\cdot}H_2O\ (crystal)} \xrightarrow{70-120\ ^\circ\mathrm{C}} \mathrm{EM\ (amorphous)} + \mathrm{H_2O\ (g)}$$

recrystallization:

$$\mathrm{EM\ (amorphous)} \xrightarrow{120-140\ ^\circ\mathrm{C}} \mathrm{EM\ (crystal)}$$

melting:

$$\mathrm{EM\ (crystal)} \xrightarrow{\sim 250\ ^\circ\mathrm{C}} \mathrm{EM\ (liquid)}$$

The single-crystal structure of EM dihydrate[33] has four water molecules per asymmetric unit, with the following two types of intermolecular hydrogen bond interactions, as shown in Table 1: (a) each oxygen atom in each water molecule forms a hydrogen bond with the hydrogen atom on the carboxyl group of the same asymmetric unit; and (b) each hydrogen atom in each water molecule forms a hydrogen bond with the oxygen atom on the mesylate anion either within the same or in the neighboring unit cell. Each of the four different water molecules forms two or three hydrogen bonds. The hydrogen bond lengths and angles for each water molecule were calculated using Cerius^{2TM} molecular modeling software and are summarized in Table 1. The $H_2O(3)$ molecule is probably more loosely bound than the other water molecules because it forms only two hydrogen bonds, whereas the other three water molecules

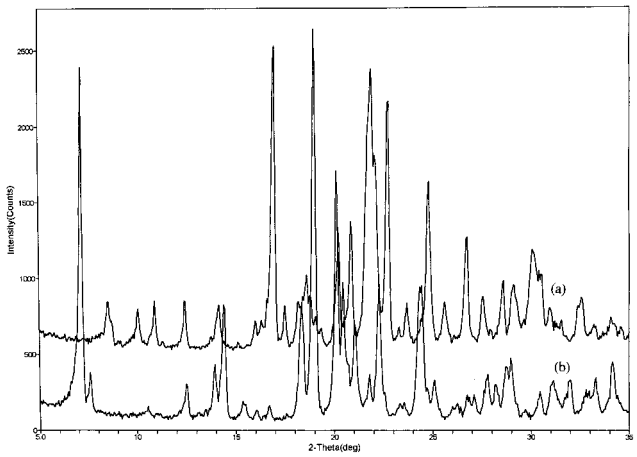

Figure 3—Typical powder X-ray diffraction patterns for eprosartan mesylate (EM): (a) dihydrate and (b) anhydrate.

form three hydrogen bonds. The $H_2O(4)$ molecule may also be more loosely bound than the $H_2O(1)$ and $H_2O(2)$ molecules because of its slightly greater hydrogen bond lengths and smaller hydrogen bond angles. Therefore, $H_2O(3)$ or $H_2O(4)$ may be included in the 1 mol of water that escapes during the first dehydration step at 25−70 °C in open-pan TGA (Figure 1a), whereas $H_2O(1)$ and $H_2O(2)$ may correspond to the second mole of water released during the second dehydration step at 70−120 °C.

Isothermal Dehydration Studies—Typical isothermal dehydration curves are shown in Figure 5 for the <125-μm sieve fraction of EM dihydrate; Figure 5a depicts the first step dehydration and Figure 5b depicts the second step dehydration. The isothermal dehydration curves for the other sieve fractions show similar features; namely, sigmoidal profiles and dehydration rates that increase with increasing temperature. The sigmoidal curves are characterized by an induction period at low x values, a growth period with an inflection at intermediate values of x, and a deceleratory period at high x values. The sigmoid-shaped curves usually result from reactions that occur at a reactant−product interface. The interface is initially established as a limited number of points on the surface of the reactant crystal by the formation of microcrystals (nuclei) of the product. Reaction thereafter proceeds within the strained contact area at the reactant−product interface. At the start of the reaction, the area of such an interface is small and limited to a number of surface sites so that the reaction is slow. At a later stage of the reaction, some nuclei have grown to a significant size and other nuclei are being formed. The reaction rate is greater than that during the initial formation of nuclei because of the increase of the reactant−product interfacial area. On continued growth of such nuclei, a point is reached at which the reactant−product interfaces from different nuclei begin to overlap so that the rate of expansion of the interface and the rate of reaction decrease.[19]

For the <125-μm fraction and for both the first and second dehydration steps, Table 2 shows that the Avrami−Erofeev equation (A3, $n = 1/3$) gave the smallest S, whereas the s_e values were randomly distributed without a trend and R^2 was largest. Thus, the successive dehydrations of the <125-μm fraction of EM dihydrate best fit the Avrami−Erofeev equation ($n = 1/3$) for which Figures 6a and 6b are the representative plots.

For the 125−180-μm and 180−250-μm fractions of EM dihydrate, the statistical parameters (S and R^2) and the dehydration equations of best fit are summarized in Tables 3 and 4, respectively. These isothermal dehydration studies were carried out between 28.3 and 93.7 °C. Up to 90.8 °C, for the first and second dehydration steps of the 125−180-μm fraction, the dehydration kinetics are best represented by the equations for a phase boundary reaction, in particular R2, the two-dimensional cylindrical symmetry reaction. At 91.2 °C, corresponding to the second dehydration step, the equation of best fit is the three-dimensional nucleation-controlled equation, A3, suggesting the dominance of nucleation and growth processes at this higher temperature. Similar dehydration kinetics were observed for the 180−250-μm fraction. At temperatures <90.7 °C for the first and second dehydration steps of the 180−250-μm fraction, the dehydration kinetics are best described by R2, the two-dimensional cylindrical phase boundary reaction. At 90.7 and 93.7 °C for the second step dehydration of the 180−250-μm sieve fraction, the equation of best fit is A3. The best fitting kinetic equations for dehydration of various sieve fractions of EM dihydrate, and the s_e values (i.e., the experimental x − the predicted x), are shown in Table 5.

The previous paragraph (Table 5) shows that the dehydration kinetics of the relatively large particles (125−180-μm and 180−250-μm fractions) up to 90.7 °C most closely follows the two-dimensional phase boundary equation (R2). Indeed, visual observation of the larger crystals under HSM (Figure 4) supports this mechanism. Direct microscopic observations of single crystals of EM dihydrate showed that tiny ruptures first appeared at a few random positions on the crystal surface, indicating initial formation of the reactant−product interface. The appearance and growth of the microcrystals proceeded along the needle axis of the crystals. The growth rate of these centers perpendicular to the needle-axis was slower than that along the needle-axis, indicating that the water molecules escape along this long axis during dehydration. The needle shape of the crystals was retained even after completion of the dehydration at the higher temperatures. This observation suggests that the dehydration reaction is confined to two-dimensions rather than to three-dimensions, which was indicated by fragmentation of the larger crystals upon dehydration.

Molecular modeling simulation (Cerius^{2TM} software) was used to visualize the crystal packing and to interpret the dehydration behavior of EM dihydrate under HSM, and revealed the existence of a water channel at the molecular level. Figures 7a and 7b show the crystal packing pattern of EM dihydrate. In general, the structure of EM dihydrate, when viewed in the direction of the a axis, is composed of alternate layers of hydrophobic regions, containing aromatic rings and hydrocarbon chains, and hydrophilic regions, containing polar functional groups and water molecules that form the hydrogen-bonded networks. A discrete hydrogen-bonding tunnel lies parallel to the a crystallographic axis as presented in Figures 7a and 7b, indicating that the water channel is also parallel to the a axis. The water molecules can leave the EM dihydrate crystal along these water channels with the smallest resistance. Dehydration along other crystallographic directions (i.e., along the b and c axes) would require the water molecules to penetrate the somewhat closely packed layers of nonpolar groups along these directions, which is unlikely. Suzuki et al.[34] and Gerdil et al.[35] applied microscopic observations and crystallographic data to the dehydration of caffeine 4/5-hydrate. Scanning electron micrographs showed that the needle-shaped crystals of the anhydrous dehydrated phase of caffeine are oriented parallel to the long axis forming channel-like cavities. This arrangement is consistent with crystallographic studies that show the chains of water molecules arranged along this axis. Byrn[7] reported that the tunnels of water molecules in thymine hydrate are oriented along the c crystallographic axis, and that rapid dehydration is consistent with the preferential exit of water molecules through these tunnels. We note that

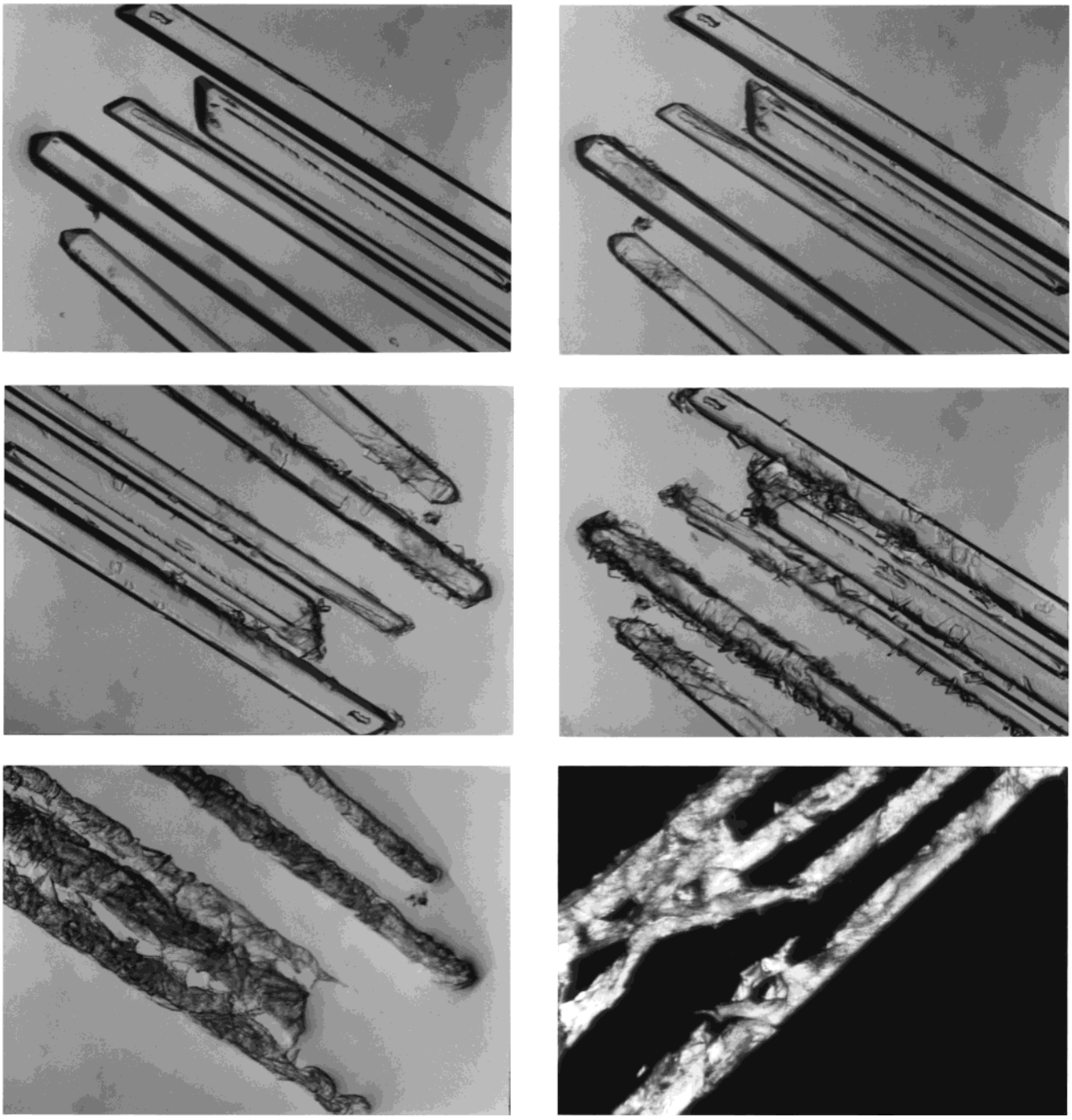

Figure 4—Photomicrographs of eprosartan mesylate (EM) dihydrate crystals while heating on the hot stage microscope at (a) 25 °C, (b) 61.0 °C, (c) 63.5 °C, (d) 65.5 °C, (e) 80.0 °C, and (f) 150 °C under polarized light.

Table 1—The Hydrogen Bond Lengths and Angles of the Four Water Molecules in the Asymmetric Unit of Eprosartan Mesylate (EM) Dihydrate

molecule	$H_2O^a\cdots H–OCO$ (Å)	bond angle (°)	$HO–H^b\cdots OSO_2CH_3$ (Å)	bond angle (°)	$HO–H^b\cdots OSO_2CH_3$ (Å)	bond angle (°)
$H_2O(1)$	2.588(9)	168.212(7)	2.823(2)	166.451(3)	2.887(3)	178.051(8)
$H_2O(2)$	2.575(0)	168.213(8)	2.878(0)	168.259(0)	2.963(2)	159.609(5)
$H_2O(3)$	2.635(3)	167.434(1)	2.783(8)	137.460(9)	—[c]	—[d]
$H_2O(4)$	2.616(6)	160.932(4)	2.802(7)	162.035(4)	2.749(7)	150.544(9)

[a] and [b] represent two different hydrogen bonds within one water molecule. [c] Distance is >4.0 Å, suggesting insignificant hydrogen bonding. [d] Bond angle is <90.0°, suggesting insignificant hydrogen bonding.

many of these hydrates crystallize with the long crystal axis parallel to the water tunnels and nearly perpendicular to the aromatic rings.

The kinetic equations of best fit for the first and second isothermal dehydration steps of three sieve fractions of EM dihydrate differ somewhat at different temperatures (Table 5). For the <125-μm fraction, the A3 equation (three-dimensional growth of nuclei) may arise from the greater total surface area or from the greater surface-to-volume ratio of these smaller crystals because nucleation is fre-

Table 2—Statistical Parameters for Fitting the First and Second Isothermal Dehydration Steps of Eprosartan Mesylate (EM) Dihydrate (<125-μm Sieve Fraction) to Eleven Solid-State Reaction Equations[a]

temperature (°C)	range of x		P1	A2	A3	F1	R1	R2	R3	D1	D2	D3	D4
					first dehydration step								
28.2	0.0621–	R^2	0.9856	0.9946	**0.9985**[b]	0.9225	0.9456	0.9942	0.9931	0.9716	0.9757	0.9081	0.9656
	0.9845	S	0.3637	0.2284	**0.2070**[b]	0.8455	0.7919	0.2305	0.2520	0.5114	0.4727	0.9210	0.5630
30.7	0.0569–	R^2	0.9813	0.9870	**0.9962**	0.8997	0.9477	0.9954	0.9864	0.9760	0.9693	0.8799	0.9517
	0.9900	S	0.3365	0.2610	**0.1555**	0.7800	0.5631	0.1666	0.2867	0.3811	0.4312	0.8537	0.5412
32.6	0.0292–	R^2	0.9680	0.9807	**0.9950**	0.8675	0.9656	0.9958	0.9742	0.9710	0.9501	0.8403	0.9253
	0.9968	S	0.3371	0.2620	**0.1368**	0.7924	0.4032	0.1982	0.3492	0.3705	0.4860	0.8699	0.5947
33.4	0.0419–	R^2	0.9941	0.9967	**0.9993**	0.9276	0.9735	0.9977	0.9852	0.9791	0.9551	0.8689	0.9327
	0.9940	S	0.1448	0.1279	**0.1489**	0.5854	0.3542	0.1443	0.2640	0.3146	0.4610	0.7880	0.5646
					second dehydration step								
75.7	0.0913–	R^2	0.9363	0.9933	**0.9983**[b]	0.9251	0.9653	0.9985	0.9889	0.9816	0.9535	0.9364	0.9479
	0.9848	S	0.5203	0.4006	**0.2929**[b]	1.3485	0.9173	0.2031	0.0906	0.3791	0.4510	0.5271	0.4770
83.8	0.0341–	R^2	0.9364	0.9655	**0.9901**	0.8161	0.9917	0.9744	0.9422	0.9531	0.8520	0.8282	0.8440
	0.9900	S	0.3177	0.0333	**0.1879**	0.2211	0.1719	0.1769	0.1916	0.3723	0.4022	0.4334	0.4129
88.9	0.0536–	R^2	0.9765	0.9840	**0.9979**	0.8811	0.9940	0.9729	0.9507	0.9418	0.8896	0.7842	0.8570
	0.9500	S	0.0827	0.1321	**0.0475**	0.3605	0.0808	0.1719	0.2320	0.2520	0.3473	0.4857	0.3953
95.0	0.0347–	R^2	0.9503	0.9623	**0.9922**	0.8222	0.9844	0.9567	0.9257	0.9249	0.8753	0.7508	0.8400
	0.9861	S	0.08264	0.1284	**0.0622**	0.2786	0.0823	0.1375	0.1416	0.1812	0.2335	0.3301	0.2645

[a] Garner[18] and Sharp et al.[25] [b] The statistical parameters for the best fitting kinectic equation are in bold.

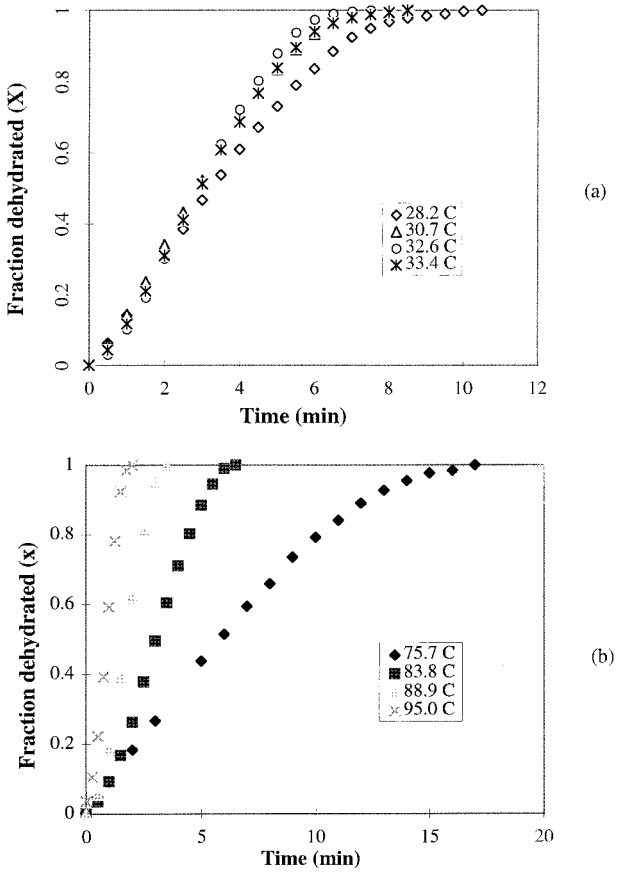

Figure 5—Representative isothermal dehydration progress curves for < 125-μm sieve fraction of eprosartan mesylate (EM) dihydrate powder during (a) the first dehydration step and (b) the second dehydration step.

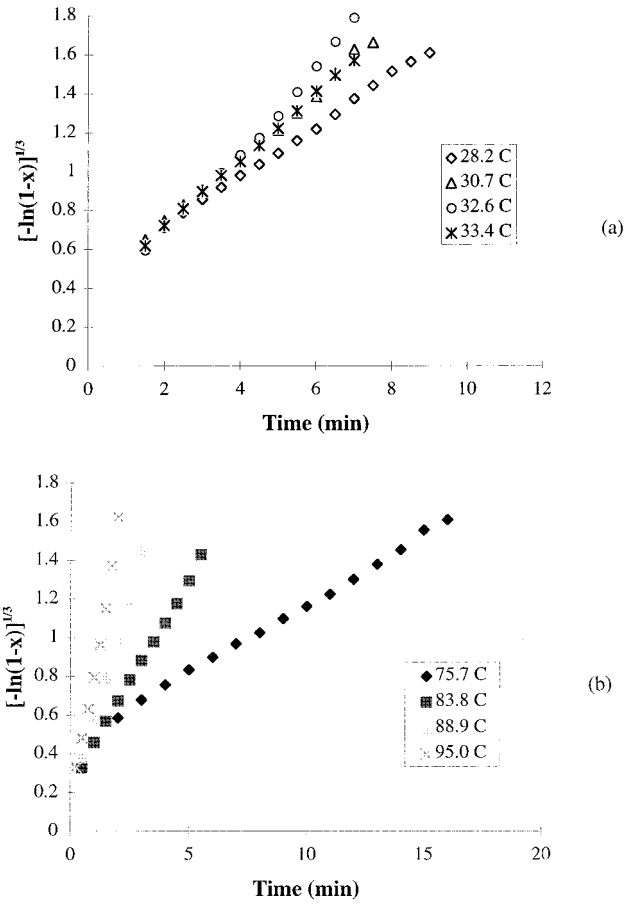

Figure 6—Representative plots for the best-fitting kinetic equation for the dehydration of eprosartan mesylate (EM) dihydrate powder (<125-μm sieve fraction) during (a) the first dehydration step and (b) the second dehydration step.

quently initiated at the crystal surfaces. The A3 equation may also arise from the greater fraction of the more reactive zones of the smaller particles (i.e., the crystal faces, edges, corners, and cracks). The smaller crystals usually have more lattice imperfections on their surfaces, which are believed to be more reactive chemically than the more perfect crystalline faces of the larger crystals. The initial generation of the small product nuclei may be a difficult process that can occur only at a limited number of the reactive sites on the crystal surface. Reaction may thereafter proceed with greater facility at the reactant−product interface. Griesser and Burger[36] reported that the dehydration of caffeine 4/5-hydrate is controlled by nucleation and growth for the smaller crystals but by diffusion for the larger crystals. In the dehydration of the larger EM dihydrate crystals (125−180 μm and 180−250 μm) at lower temperatures, the escape of water molecules from the crystal lattice follows the R2 equation (two-dimensional

Table 3—Statistical Parameters for Fitting the Isothermal Dehydration Steps of Eprosartan Mesylate (EM) Dihydrate (125–180-μm Sieve Fraction) to Eleven Solid-State Reaction Equations[a]

temperature (°C)	range of x		P1	A2	A3	F1	R1	R2	R3	D1	D2	D3	D4
first dehydration step													
28.3	0.1156–	R^2	0.9857	0.9958	0.9957	0.9541	0.9854	**0.9980**[b]	0.9922	0.9899	0.9600	0.8837	0.9381
	0.9827	S	0.2929	0.1524	0.2082	0.5664	0.3192	**0.1421**[b]	0.0976	0.2649	0.5290	0.9021	0.6580
30.8	0.0561–	R^2	0.8837	0.9716	0.9902	0.8602	0.9631	**0.9972**	0.9793	0.9441	0.9201	0.8888	0.9100
	0.9971	S	0.2376	0.0508	0.1368	0.1864	0.0395	**0.1220**	0.0905	0.3127	0.3737	0.4409	0.3968
33.2	0.1540–	R^2	0.9364	0.9876	0.9957	0.9136	0.9629	**0.9974**	0.9852	0.9559	0.9267	0.8833	0.9129
	0.9811	S	0.2525	0.0586	0.1054	0.2094	0.5135	**0.0818**	0.0909	0.2778	0.3581	0.4518	0.3903
34.8	0.1038–	R^2	0.9572	0.9890	0.9926	0.9213	0.9581	**0.9937**	0.9845	0.9435	0.9141	0.8702	0.9002
	0.9937	S	0.3397	0.1698	0.1536	0.2375	0.1707	**0.1502**	0.1964	0.3141	0.3877	0.4765	0.4179
second dehydration step													
75.4	0.0647–	R^2	0.8871	0.9748	0.9906	0.8751	0.9711	**0.9967**[b]	0.9780	0.9912	0.9717	0.8507	0.9438
	0.9935	S	0.9240	0.7283	0.4778	1.7416	0.8376	**0.2845**[b]	0.7304	0.4610	0.8293	1.9039	1.1678
81.7	0.1634–	R^2	0.8488	0.9594	0.9831	0.8325	0.9724	**0.9938**	0.09659	0.9836	0.9547	0.8140	0.9218
	0.9967	S	0.5248	0.4385	0.2833	0.9498	0.3501	**0.1716**	0.4287	0.2966	0.4939	1.0006	0.6491
90.8	0.3101–	R^2	0.7993	0.9318	0.9610	0.8104	0.9796	**0.9905**	0.9513	0.8586	0.8643	0.8067	0.8251
	0.9968	S	0.2351	0.1918	0.1444	0.3187	0.1045	**0.0712**	0.1305	0.2224	0.2408	0.2601	0.2474
93.6	0.0671–	R^2	0.9570	0.9755	**0.9971**[b]	0.9597	0.9753	0.9440	0.9246	0.9929	0.9928	0.8938	0.9937
	0.9840	S	0.0706	0.1928	**0.0578**[b]	0.1298	0.6692	0.0733	0.9208	0.9921	0.9901	0.0818	0.9934

[a] Garner[18] and Sharp et al.[25] [b] The statistical parameters for the best fitting kinectic equation are in bold.

Table 4—Statistical Parameters for Fitting the Isothermal Dehydration Steps of Eprosartan Mesylate (EM) Dihydrate (180–250-μm Sieve Fraction) to Eleven Solid-State Reaction Equations[a]

temperature (°C)	range of x		P1	A2	A3	F1	R1	R2	R3	D1	D2	D3	D4
first dehydration step													
28.3	0.0427–	R^2	0.8910	0.9774	0.9901	0.8581	0.9663	**0.9971**[b]	0.9791	0.9837	0.9644	0.8388	0.9375
	0.9970	S	0.5816	0.4569	0.3019	1.1447	0.5583	**0.1633**[b]	0.4395	0.3885	0.5731	1.2201	0.7596
30.8	0.0372–	R^2	0.9344	0.9928	0.9979	0.9055	0.9659	**0.9990**	0.9913	0.9867	0.9836	0.8996	0.9669
	0.9907	S	0.3341	0.2212	0.1060	0.8016	0.4810	**0.0689**	0.2161	0.2676	0.2976	0.7354	0.4216
32.4	0.1032–	R^2	0.8609	0.9614	0.9839	0.8273	0.9715	**0.9956**	0.9714	0.9882	0.9660	0.8198	0.9347
	0.9968	S	0.4886	0.3898	0.2735	0.8452	0.3436	**0.1354**	0.3440	0.2211	0.3749	0.8634	0.5197
34.9	0.0856–	R^2	0.9477	0.9935	0.9971	0.9276	0.9761	**0.9961**	0.9829	0.9851	0.9596	0.8629	0.9346
	0.9939	S	0.3749	0.1692	0.1022	0.5501	0.2925	**0.1181**	0.2471	0.2310	0.3799	0.7001	0.4837
second dehydration step													
76.5	0.0854–	R^2	0.8423	0.9602	0.9821	0.8454	0.9687	**0.9962**[b]	0.9743	0.9923	0.9758	0.8453	0.9480
	0.9968	S	1.1447	0.9258	0.6204	1.8247	0.8207	**0.2853**[b]	0.4219	0.4081	0.7212	1.8254	1.058
83.2	0.0521–	R^2	0.8538	0.9588	0.9836	0.8294	0.9744	**0.9937**	0.9686	0.9869	0.9639	0.8223	0.9329
	0.9967	S	0.4546	0.3839	0.2419	0.7810	0.3024	**0.1499**	0.3350	0.2164	0.3588	0.7971	0.4898
90.7	0.0444–	R^2	0.8868	0.9922	**0.9979**[b]	0.9307	0.9600	0.9902	0.9829	0.9732	0.9616	0.8929	0.9457
	0.9905	S	0.0777	0.0836	**0.0432**[b]	0.2488	0.3206	0.0936	0.1234	0.2514	0.2164	0.2863	0.2167
93.7	0.0477–	R^2	0.9496	0.9834	**0.9952**	0.9043	0.9800	0.9867	0.9651	0.9346	0.9319	0.8946	0.9255
	0.9809	S	0.0573	0.0762	**0.0456**	0.1830	0.0837	0.0756	0.1501	0.2054	0.2095	0.2606	0.2191

[a] Garner,[18] and Sharp etal.[25] [b] The statistical data for the best fitting kinectic equation are in bold.

Table 5—The Best-Fitting Kinetic Equations at Various Temperatures for the First and Second Isothermal Dehydrations of All the Eprosartan Mesylate (EM) Dihydrate Samples

	< 125 μm			125–180 μm			180–250 μm		
dehydration	temperature (°C)	equation[a]	residual plots[b]	temperature (°C)	equation[a]	residual plots[b]	temperature (°C)	equation[a]	residual plots[b]
first	28.2	A3	no trend	28.3	R2	no trend	28.3	R2	no trend
	30.7	A3	no trend	30.8	R2	no trend	30.8	R2	no trend
	32.6	A3	no trend	33.2	R2	no trend	32.4	R2	no trend
	33.4	A3	no trend	34.8	R2	no trend	34.9	R2	no trend
second	75.6	A3	no trend	75.4	R2	no trend	76.5	R2	no trend
	83.8	A3	no trend	81.7	R2	no trend	83.2	R2	no trend
	88.9	A3	no trend	90.8	R2	no trend	90.7	A3	no trend
	95.0	A3	no trend	93.6	A3	no trend	93.7	A3	no trend

[a] Garner[18] and Sharp et al.[25] [b] The residual plots of the residuals, s_e (i.e., the experimental x – the predicted x), versus the predicted x at different dehydration times, t.

phase boundary reaction). The explanation offered is that the escape of the loosely bound water molecules in the crystal lattice produces a vacancy on the surface of the EM dihydrate crystals. This intermediate structure is unstable, so recrystallization to the anhydrous phase occurs. In this way, a phase boundary is formed that is preferentially oriented along the a axis inside the crystal. At higher temperatures, the large EM dihydrate particles can presumably break up to produce smaller crystals. A large number of reactive crystal defects, which are the initial sites for the nucleation, are presumably produced by the fragmentation of the larger particles into smaller ones.

Table 6—The Activation Energy (E_a, kcal/Mol) and Frequency Factors (A, min) from Arrhenius Plots for the Dehydration of Eprosartan Mesylate (EM) Dihydrate Samples of various particle size ranges

	< 125 μm		125–180 μm		180–250 μm	
parameter	first dehydration	second dehydration	first dehydration	second dehydration	first dehydration	second dehydration
E_a (kcal/mol)	18.9 (0.2)[a]	31.9 (0.6)[a]	19.2 (0.5)	31.1 (0.5)	19.1 (0.6)	35.1 (0.5)
ln A (min)	29.5	43.4	29.8	42.1	29.8	48.2

[a] The standard deviations are given in parentheses.

Table 7—The Activation Energy (E_a, kcal/mol) and Frequency Factors (A, min) from Kissinger Plots for the First and Second Dehydrations of Eprosartan Mesylate (EM) Dihydrate Samples of Various Particle Sizes and from Various Preparation Methods[a]

	preparation methods						
	98% RH		slurry process			with 3% corn starch	
dehydration step	< 125 μm	125–180 μm	< 125 μm	125–180 μm	180–250 μm	125–180 μm	180–250 μm
first, E_a (kcal/mol)	18.5(0.6)	19.6(0.8)	12.0(0.2)	11.8 (0.1)	12.3(0.3)	13.6(0.3)	14.5(0.5)
second, E_a (kcal/mol)	33.9(1.1)	31.4(0.8)	20.9(0.8)	18.7(0.5)	23.4(0.6)	38.9(0.9)	29.6(0.3)
first, ln A (min)	30.0	32.2	18.9	18.4	19.2	20.8	23.0
second, ln A (min)	43.0	43.8	28.9	25.8	32.5	53.4	39.7

[a] The standard deviations are given in parentheses.

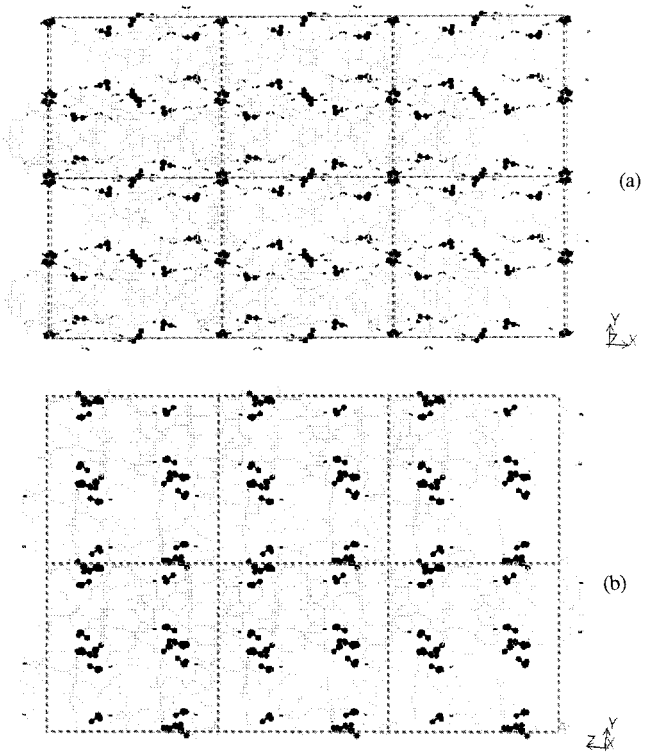

Figure 7—Packing diagrams of eprosartan mesylate (EM) dihydrate, where the dotted lines between the atoms indicate the hydrogen bonds along (a) the *a* axis and (b) the *c* axis.

Hence, for the larger crystals, the dominant dehydration process (two-dimensional phase boundary, R2, cylindrical symmetry) at low temperatures is replaced by three-dimensional nucleation-controlled (A3) dehydration at high temperatures because of the creation of increased surface area and crystal defects at high temperatures, which are the reactive sites for the formation of nuclei.

For the first and second dehydration steps of EM dihydrate, the activation energies, E_a, obtained from Arrhenius plots (Figure 8) and the frequency factors according to the best-fitting mechanism are presented in Table 6. In all cases, E_a for the second dehydration step (~32 kcal/mol) is higher than that for the first step (~19 kcal/mol), which indicates that the second mole of escaping water molecules is more tightly bound. This conclusion agrees

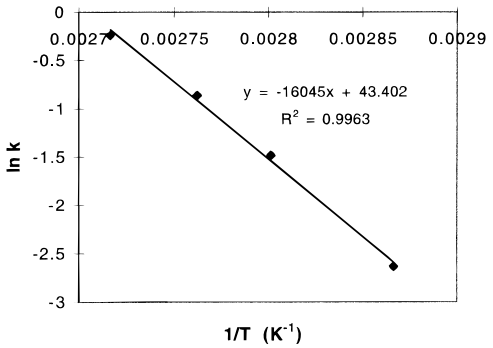

Figure 8—Arrhenius plot from the best-fitting dehydration mechanism for the second dehydration step of eprosartan mesylate (EM) dihydrate samples (<125-μm sieve fraction).

with that from the study of the bonding environment of water molecules in EM dihydrate, already discussed. Neither the activation energy nor the frequency factor depend significantly on the particle size. However, Agbada and York[21] and Van Dooren[37] reported the tendency toward lower activation energy with decreasing particle size for the dehydration of theophylline monohydrate and sodium citrate.

Nonisothermal Dehydration Studies—For the EM dihydrate samples prepared by different methods, the activation energies and the frequency factors of the first and second dehydration steps were calculated from the Kissinger plots of DSC data and are listed in Table 7. The activation energies for dehydration of the EM dihydrate samples depend on the method of preparation and increase in the following order: slurry process < 98% RH < in the presence of 3% corn starch. The dependence of the activation energy of dehydration on the manufacturing process suggests the influence of variables, such as crystals defects, sample geometry, and surface characteristics, on the properties of the crystals. Similarly, Agbada and York[21] noted that the sample history plays a critical role in the dehydration reactions of theophylline monohydrate.

Conclusions

The two consecutive dehydration reactions of EM dihydrate are complex and represent different kinetic processes that are greatly dependent on the particle size and tem-

perature. Both three-dimensional growth of nuclei and two-dimensional phase boundary equations are postulated to represent the predominant processes in the dehydration kinetics of EM dihydrate. Such information is essential for understanding and improving the stability of EM dihydrate, which may be compromised during the processes of manufacture and storage. In addition, the activation energies for the two consecutive dehydration processes of EM dihydrate depend on the sample preparation history. HSM and variable temperature PXRD are valuable complementary tools for the interpretation of dehydration behavior, whereas molecular modeling provides structural insight into the dehydration mechanisms.

Acknowledgments

We thank the following: Dr. Victor G. Young, Jr., for solving the crystal structure of eprosartan mesylate dihydrate (ref 33) on which Figure 7 and associated discussion is based; Geoff G. Z. Zhang and Linna R. Chen for helpful discussions; SmithKline Beecham Pharmaceuticals, King of Prussia, PA, for financial support and for supplying eprosartan mesylate; and the Supercomputing Institute of the University of Minnesota for financially supporting our use of the Medicinal Chemistry/Supercomputing Institute Visualization−Workstation Laboratory.

References and Notes

1. Khankari, R. H.; Grant, D. J. W. Pharmaceutical hydrates. *Thermochim. Acta*. **1995**, *248*, 61−79.
2. Haleblian, J. Characterization of habits and crystalline modification of solids and their pharmaceutical applications. *J. Pharm. Sci.* **1975**, *64*, 1269−1288.
3. *The United State Pharmacopeia, The National Formulary*; United States Pharmacopeial Convention, Inc.: Rockville, MD; 1995.
4. *European Pharmacopoeia*. 3rd ed., Council of Europe: Strasbourg, France, 1996.
5. Burger, A. Das Auflösungsverhalten von Sulfanilamid in Wasser. *Pharm. Ind*. **1973**, *35*, 626−633.
6. Burger, A.; Griesser, U. J. Physical stability, hygroscopicity and solubility of succinyl-sulfathiazole. *Eur. J. Pharm. Biopharm*. **1991**, *37*, 118−124.
7. Byrn, S. R. *Solid-State Chemistry of Drugs*, Academic: New York, 1982; pp 59−74, 149−186.
8. Ando, H.; Ohwaki, T.; Ishii, M.; Watanabe, S.; Miyake, Y. Crystallization of theophylline in tablets. *Int. J. Pharm*. **1986**, *34*, 153−156.
9. Chowhan, Z. T. Physical paths of instability. *Pharm. Technol.* **1982**, *6*, 47−48.
10. Brittain, H. G.; Bugay, D. E.; Bogdanowich, S. J.; DeVincentis, J. Spectral methods for determination of water. *Drug. Dev. Ind. Pharm*. **1988**, *14*, 2029−2046.
11. Giron, D. Thermal analysis and calorimetric methods in the characterization of polymorphs and solvates. *Thermochim. Acta* **1995**, *248*, 1−59.
12. Jaffé, J.; Foss, N. E. Compression of crystalline substances. *J. Am. Pharm. Assoc. Sci. Ed.* **1959**, *48*, 26−29.
13. Shefter, E.; Higuchi, T. Dissolution behaviour of crystalline solvated and nonsolvated forms of some pharmaceuticals. *J. Pharm. Sci.* **1963**, *52*, 781−791.
14. Poole, J. W.; Owen, G.; Silverio, J.; Freyholf, J. N.; Rosenman, S. B. Physicochemical factors influencing the absorption of anhydrous and trihydrate forms of ampicillin. *Curr. Ther. Res*. **1968**, *10*, 292−303.
15. Lerk, C. F.; Andreae, A. C.; Bolhuis, G. K.; Zuurman, K.; Hoog, P.; Kussendrager, K.; Leverink, J. V. Increased binding capacity and flowability of α-lactose monohydrate after dehydration. *J. Pharm. Pharmacol.* **1983**, *35*, 747−748.
16. Lerk, C. F.; Zuurman, K.; Kussendrager, K. Effect of dehydration on the binding capacity of particulate hydrates. *J. Pharm. Pharmacol.* **1984**, *36*, 399.
17. Otsuka, M.; Kaneniwa, N. Dehydration of cephalexin hydrates. *Chem. Pharm. Bull.* **1983**, *31*, 1021−1029.
18. *Chemistry of the Solid State*; Garner, W. E., Ed.; Academic: New York, NY, 1955; pp 232−253.
19. Galwey, A. K. *Chemistry of Solids*. Chapman and Hall: London, UK, 1967; pp 163−195.
20. Carstensen, J. T. *Drug Stability*: *Principles and Practice*, 2nd ed.; Marcel Dekker: New York, 1995; pp 230−280.
21. Agbada, C. O.; York, P. Dehydration of theophylline monohydrate powder—effects of particle size and sample weight. *Int. J. Pharm*. **1994**, *106*, 33−40.
22. Chen, L.; Grant, D. J. W. *Dehydration of Nedocromil Sodium Trihydrate*, College of Pharmacy, University of Minnesota, Minneapolis, MN, Personal Communication, 1996.
23. Monkhouse, D. C.; Campen, L. V. Solid-state reactions—theoretical and experimental aspects. *Drug. Dev. Ind. Pharm*. **1984**, *10*, 1175−1276.
24. Criado, J. M.; Morales, J.; Rivers, V. Computer kinetic analysis of simultaneously obtained TG and DTG curves. *J. Therm. Anal.* **1978**, *14*, 221−228.
25. Sharp, J. H.; Brindley, G. W.; Achar, B. N. N. Numerical data for some commonly used solid-state reaction equations. *J. Am. Ceram. Soc.* **1966**, *49*, 379−382.
26. Davis, W. H. J.; Pryor, W. A. Measures of goodness of fit in linear free energy relationships. *J. Chem. Educ.* **1976**, *53*, 285−287.
27. Brown, M. E.; Galwey, A. K. The distinguishability of selected kinetic models for isothermal solid-state reactions. *Thermochim. Acta* **1979**, *29*, 129−146.
28. Duddu, S. P.; Venkatesh, G. M.; Palepu, N. R. *Effect of excipients on the solid-state conversion of SK&F 108566-J into its hydrated form in the presence of water.* SmithKline Beecham Pharmaceuticals, King of Prussia, PA; *Report*, 1996.
29. Venkatesh, G. M. *SK&F 108566-J: Hydrate Formation − Further Studies*. SmithKline Beecham Pharmaceuticals, King of Prussia, PA; *Report*, 1996.
30. Sheng, J.; Duddu, S. P.; Venkatesh, G. M.; Palepu, N. R.; Zell, M. T.; Munson, E. J.; Grant, D. J. W. Dehydration behavior of eprosartan mesylate dihydrate. *Pharm. Res. Suppl.* **1997**, *14*, S-493, 3092.
31. Sheng, J.; Zhang, G.; Young, V. G.; Duddu, S. P.; Venkatesh, G. M.; Palepu, N. R.; Grant, D. J. W. Phase transformation and the single-crystal structure of SKF 108566-J dihydrate. *Pharm. Res. Suppl.* **1997**, *14*, S-492, 3091.
32. Kissinger, H. E. Reaction kinetics in differential thermal analysis. *Anal. Chem*. **1957**, *29*, 1702−1706.
33. Sheng, J.; Young, V. G., Jr.; Haltwanger, R. C.; Eggleston, D. S.; Grant, D. J. W. Crystal structure of eprosartan mesylate dihydrate and its comparison with that of eprosartan mesylate anhydrate, manuscript in preparation.
34. Suzuki, E.; Shirotani, K.; Tsuda, Y.; Sekiguchi, K. Studies on methods of particle size reduction of medicinal compounds: XXII. Water content and dehydration behaviour of crystalline caffiene hydrate. *Chem. Pharm. Bull.* **1985**, *33*, 5028−5035.
35. Gerdil, R.; Marsh, R. E. On the arrangement of water molecules in the crystal structure of caffeine. *Acta Crystallogr.* **1960**, *13*, 166−167.
36. Griesser, U. J.; Burger, A. The effect of water vapor pressure on desolvation kinetics of caffeine 4/5-hydrate. *Int. J. Pharm*. **1995**, *120*, 83−93.
37. Van Dooren, A. A. *Effect of operational factors on kinetic parameters determined with DSC*. Proc. 7th. Int. Conf. on Thermal Analysis; Wiley: Chichester, UK, 1982; pp 80−84.

JS9900250